RESEARCH ARTICLE | JANUARY 25 2021

Nanoscale imaging of Gilbert damping using signal amplitude mapping

Guanzhong Wu ; Yang Cheng; Side Guo; Fengyuan Yang ; Denis V. Pelekhov; P. Chris Hammel

Appl. Phys. Lett. 118, 042403 (2021)
https://doi.org/10.1063/5.0023455

Applied Physics Letters ARTICLE scitation.org/journal/apl

Nanoscale imaging of Gilbert damping using signal amplitude mapping

Cite as: Appl. Phys. Lett. **118**, 042403 (2021); doi: 10.1063/5.0023455
Submitted: 29 July 2020 · Accepted: 14 January 2021 ·
Published Online: 25 January 2021

Guanzhong Wu,[a] Yang Cheng, Side Guo, Fengyuan Yang, Denis V. Pelekhov, and P. Chris Hammel

AFFILIATIONS

Department of Physics, The Ohio State University, Columbus, Ohio 43210, USA

[a]Author to whom correspondence should be addressed: wu.2314@osu.edu

ABSTRACT

Ferromagnetic resonance force microscopy (FMRFM) is a powerful scanned probe technique that uses sub-micrometer-scale, spatially localized standing spin wave modes (LMs) to perform local ferromagnetic resonance (FMR) measurements. Here, we show the spatially resolved imaging of Gilbert damping in a ferromagnetic material (FM) using FMRFM. Typically damping is measured from the FMR linewidth. We demonstrate an approach to image the spatial variation of Gilbert damping utilizing the LM resonance peak height to measure the LM resonance cone angle. This approach enables determination of damping through field-swept FMRFM at a single excitation frequency. The extreme force sensitivity of ∼2 fN at room temperature can resolve changes of Gilbert damping as small as $\sim 2 \times 10^{-4}$ at 2 GHz, corresponding to ∼0.16 Oe in FMR linewidth resolution. This high sensitivity, high spatial resolution, and single frequency imaging of Gilbert damping creates the opportunity to study spin interactions at the interface between an insulating FM and a small volume of nonmagnetic material such as atomically thin two-dimensional materials.

Magnetic resonance imaging (MRI) enables the study of spin interactions and spin dynamics with spatial resolution unavailable through bulk magnetic resonance measurements that are based on the measurement of the global absorption of radio frequency (RF) excitation. Advances in MRI have reached the single electron scale by various techniques.[1–5] Among these, magnetic resonance force microscopy (MRFM) is well-developed and has realized imaging of a single electron spin.[6] Its close relative, ferromagnetic resonance force microscopy (FMRFM), extends the scope of nanoscale MRI to the study of ferromagnetic materials (FMs) where strong spin interactions are present.[7] We have shown that FMRFM can image internal field profiles in FM thin films using probe field localized standing spin wave modes (LMs) with an ∼100 nm spatial resolution.[8] This force-detected scanning field gradient technique does not rely on electrical current injection in the materials and, therefore, provides opportunities for the microscopic study of spin pumping and spin torques in insulating FMs.[9,10]

In this Letter, we expand the capability of FMRFM to spatially resolved imaging of Gilbert damping in a FM insulator $Y_3Fe_5O_{12}$ (YIG) thin film. When the resonance amplitude is small, and so in the linear regime, the dissipative term described by Gilbert damping contributes to the ferromagnetic resonance (FMR) linewidth,

$$\Delta H = \Delta H_{\mathrm{inh}} + 4\pi\alpha f/\sqrt{3}\gamma, \tag{1}$$

where α is the dimensionless Gilbert damping constant, f the RF excitation frequency, γ the gyromagnetic ratio, and ΔH_{inh} the inhomogeneous broadening. Gilbert damping is generally inferred from the frequency dependence of the FMR linewidth, assuming ΔH_{inh} is frequency independent.[11]

However, this broadband FMR measurement routine introduces significant difficulty in FMRFM spatially resolved imaging. A key issue is the systematic linewidth broadening due to cantilever oscillation, which will be discussed in detail later. Here, we demonstrate an approach to achieve spatially resolved imaging of Gilbert damping using the LM resonance amplitude in the FMRFM spectrum. Our approach focuses on the resonance cone angle of the LM since it determines the dipolar force applied on the cantilever tip and, hence, the signal amplitude in the FMRFM spectrum. It is also applicable to many other scanned probe techniques since, in many cases, the resonance cone angle is directly related to the signal amplitude. This approach can resolve Gilbert damping variation as small as $\sim 2.0 \times 10^{-4}$ with sub-micrometer spatial resolution in a field-swept FMRFM measurement performed at a single excitation frequency. It offers immediate application in studying spin dynamics and interfacial spin interactions in mesoscopic samples such as van der Waals heterostructures containing ferromagnetic materials.[12–16]

FMRFM uses LMs confined by a strong probe field to accomplish FMR imaging [Fig. 1(a)]. The measurements below are performed with an external magnetic field oriented out of the sample plane. These LMs resemble the standing spin wave modes found in a perpendicularly magnetized FM disk[17] with different radii associated with various LM indices. We use the $n = 1$ LM for spatially resolved imaging since it has the smallest mode radius and can achieve the highest spatial resolution [Fig. 1(a)]. We acquire FMRFM spectra at a constant RF excitation frequency while sweeping the external magnetic field. The cantilever is continuously driven by a piezoactuator at the cantilever fundamental frequency $f_c \approx 19$ kHz and its oscillation amplitude is monitored by fiber interferometry and measured as a lock-in voltage signal A. When the resonance condition for the LM is met, the out-of-plane magnetization $\vec{M}_z$ is locally reduced, altering the magnetic dipolar force $\vec{F}_{LM}$ exerted on the tip. We modulate the RF excitation amplitude at f_c and tune its phase relative to the cantilever displacement to generate the largest signal amplitude [Fig. 1(b)]. In this case, $\vec{F}_{LM}$ drives the cantilever along with the piezoactuator, thereby increasing the signal amplitude by $\Delta A = A_{on} - A_{off}$, where A_{off} is the off resonance amplitude when driven solely by the piezoactuator and A_{on} is the on-resonance amplitude driven by the combination of piezoactuator and modulated dipolar field from the LM. Due to the reduced active area in FMRFM detection and the capability of imaging spatial variation of resonance field with high spatial and spectral resolution, it is possible to find a uniform region in the sample and eliminate inhomogeneous broadening contribution to the linewidth. However, in the following, we will discuss another important source of resonance line broadening, ΔH_{osc}, due to the cantilever oscillation.

A low damping YIG thin film is used in our experiment since multiple LMs can be resolved.[18] Figure 1(c) shows several FMRFM spectra measured on a YIG(20 nm)/$Gd_3Ga_5O_{12}$ (GGG) (111) thin film with different piezoactuator drives, and hence, different cantilever oscillation amplitudes indicated by A_{off}. The increase in the $n = 1$ LM resonance linewidth ΔH_{osc} with the cantilever oscillation amplitude is evident. The strong field spatial gradient of the dipolar magnetic field of the micromagnetic tip causes the field experienced by the sample to vary with its separation from the tip: the sample experiences a range of magnetic fields as a consequence of the oscillation of the cantilever, which broadens the FMR line. To verify this, we perform a variational calculation[8] to find the $n = 1$ LM resonance field $H_{r,1}$ at varying probe heights using parameters corresponding to the experimental conditions: tip magnetic moment $m_{prob} = 4.48$ nemu, probe sample separation $\sim 4\,\mu$m, YIG saturation magnetization $4\pi M_s = 1700$ G, YIG effective magnetization $4\pi M_{eff} = 2370$ G, YIG film thickness $t_{FM} = 20$ nm, RF excitation frequency $f = 2$ GHz, and gyromagnetic ratio $\gamma = 2\pi \times 27.958$ GHz/T. The calculation result is shown in Fig. 1(d). A 50 nm change of tip height, close to the typically used cantilever oscillation amplitude, leads to ~ 7 Oe variation of $H_{r,1}$, indicated by the blue dashed lines in Fig. 1(d). This change of $H_{r,1}$ is comparable to the intrinsic FMR linewidth of the 20 nm YIG film. Therefore, even though inhomogeneous broadening is negligible in the FMRFM measurement, we cannot rely on measurement of the LM linewidth

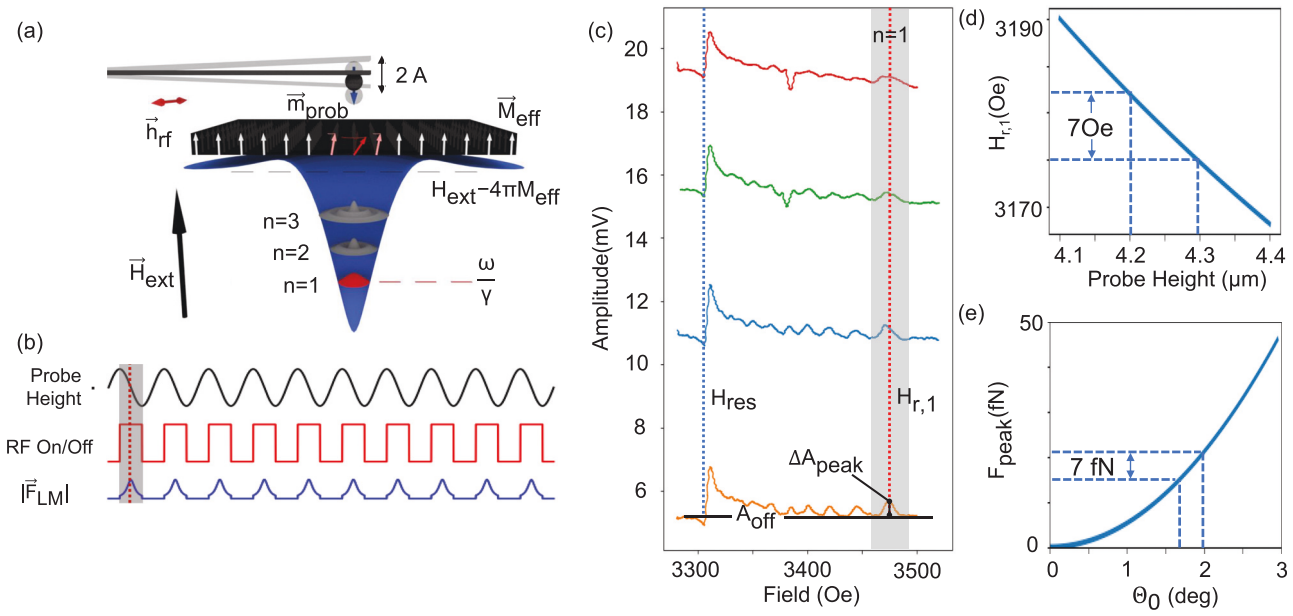

FIG. 1. FMRFM linewidth measurement and variational calculation. (a) FMRFM probe $\vec{m}_{prob}$ generates a field well immediately beneath the probe, confining multiple LMs with different radii. In this diagram, the $n = 1$ LM is on resonance driven by the transverse RF field $\vec{h}_{rf}$ at angular frequency ω. LM with index n has different resonance field $H_{r,n}$ from the uniform FMR mode resonance field H_{res}, which follows $\omega/\gamma = H_{res} - 4\pi M_{eff}$. (b) FMRFM measurement sequence. The cantilever equilibrium position is indicated by the horizontal black dashed line. The vertical red dashed line shows that the $n = 1$ LM is on-resonance at cantilever equilibrium position. In order to induce the largest on-resonance amplitude $A + \Delta A$, RF excitation phase is tuned so that $\vec{F}_{LM}$ does positive work to the cantilever at each cycle, as indicated in the gray window. (c) FMRFM spectra acquired at different off resonance cantilever oscillation amplitude A_{off}. A_{off} and ΔA_{peak} are labeled for the lowest spectrum. Broadening of the $n = 1$ LM resonance peak with increasing A_{off} is evident. (d) Variational calculation results of the $n = 1$ LM resonance field as a function of probe height. (e) Variational calculation results of the on-resonance F_{peak} as a function of resonance cone angle θ_0 at the center of the $n = 1$ LM.

obtained by sweeping field at a single RF frequency to calculate Gilbert damping. In order to find the local Gilbert damping using FMRFM, a broadband measurement needs to be done while keeping cantilever oscillation amplitude unchanged.[9,19]

Another way to measure Gilbert damping is to directly determine the cone angle of the FM resonance. In FMRFM, the LM precession cone angle determines the magnitude of $\vec{F}_{\mathrm{LM}}$, which is sensitively measured through its influence on the amplitude of cantilever oscillation $\Delta A = A_{\mathrm{on}} - A_{\mathrm{off}}$.[20] Therefore, ΔA contains information about the local Gilbert damping in the FM. We now test the validity of this experimental method for measuring damping using two theoretical approaches: (a) an analytical variational study of the relationship between the peak value LM resonance amplitude ΔA_{peak} and the local Gilbert damping α [results shown in Fig. 1(e)]; and (b) micromagnetic simulations using MuMax3[21] shown in Fig. 2. First, we perform a variational calculation using the same parameters as used in Fig. 1(d) to show the dependence of $|\vec{F}_{\mathrm{LM}}|$ on the LM resonance cone angle. Figure 1(e) shows the magnitude of F_{peak}, which denotes the peak value of $|\vec{F}_{\mathrm{LM}}|(H)$ when the $n = 1$ LM is on resonance during a field sweep as a function of resonance cone angle θ_0. Here, θ_0 is the resonance cone angle at the center of the localized mode where it reaches the maximum. Note that the minimum force detectable in our FMRFM is $F_{\mathrm{min}} \approx 2$ fN, and the 7 fN change of F_{peak} in Fig. 1(e) from less than 0.5° difference of θ_0 indicates detectable ΔA variation. We show below that ΔA is more sensitive than ΔH to Gilbert damping in the FMRFM measurement, and it is possible to achieve a single RF excitation frequency measurement of Gilbert damping, which greatly eases the process of spatially resolved imaging.

We now use micromagnetic simulation to examine the determination of damping from ΔA. In what follows, we set the RF excitation frequency and power constant and assume small on-resonance cone angle $\theta < 3°$. We calculate the peak value of the force on the cantilever $|\vec{F}_{\mathrm{LM}}|(H)$ exerted by the n_{th} LM when it is on resonance, which is termed $F_{\mathrm{peak,n}}$

$$F_{\mathrm{peak,n}} \approx \frac{1}{\alpha^2}\left[\pi M_s t_{\mathrm{FM}}\left[\frac{|\mathrm{h}_+|}{H_{\mathrm{r,n}}}\right]^2 \nabla_z B_{\mathrm{prob,z}} \int_0^{R_n} J_{0,n}\left(\frac{a_n r}{R_n}\right) r dr\right], \quad (2)$$

where h_+ is the amplitude of the right circularly polarized component of the RF field, $H_{\mathrm{r,n}}$ is the resonance field of the n_{th} LM, and $\nabla_z B_{\mathrm{prob,z}}$ is the out-of-plane component of the probe field gradient. The spatial distribution of the out-of-plane component of LM magnetization is described by $J_{0,n}(a_n r/R_n)$, the zeroth Bessel function truncated at its n_{th} zero a_n, and R_n is the radius of the n_{th} LM. Here, we focus on the $n = 1$ LM and use F_{peak} as the peak value of $|\vec{F}_{\mathrm{LM}}|$ when the $n = 1$ LM is on resonance. As shown in Fig. 1(e), $F_{\mathrm{peak}} \propto \theta_0^2$ is evident from the variational calculation. And using $\theta_0 = |\mathrm{h}_+|/\alpha H_{\mathrm{res}}$, $F_{\mathrm{peak}} \propto 1/\alpha^2$ in Eq. (2) is confirmed. To further corroborate Eq. (2), we perform MuMax3 simulation on $|\vec{F}_{\mathrm{LM}}|(H)$ centered around the $n = 1$ LM resonance field $H_{\mathrm{r,1}}$ using the same parameters as used in the variational calculation. Figure 2(a) shows the simulated $|\vec{F}_{\mathrm{LM}}|(H)$ near resonance for several values of α. The calculated F_{peak} decreases rapidly as α increases. Comparison with Fig. 1(e) shows that the value of F_{peak} is in the regime of small cone angle $\theta_0 < 3°$. In Fig. 2(b), we show the linear relationship between F_{peak} and $1/\alpha^2$, consistent with our theoretical conclusion in Eq. (2). Therefore, this shows that the measured resonance peak amplitude $\Delta A_{\mathrm{peak}} \propto 1/\alpha^2$.

Building on this theoretical foundation, we obtain the Gilbert damping α by measuring the peak amplitude ΔA_{peak} of the LM resonance. We note that this approach of determining the local damping α at a specific location relies on the knowledge of the LM damping in the reference area α_{ref}, which is assumed to be equal to the broadband FMR measured value, and then this approach measures the change in α at the target location relative to the reference location. Therefore, this measurement scheme requires uniform M_s and FM thickness t_{FM} in the scanned area since they affect the value of $|\vec{F}_{\mathrm{LM}}|$ and is suitable for measuring Gilbert damping in a heterostructure composed of a FM thin film and a micrometer-sized nonmagnetic material (NM) layer. We choose a 20 nm YIG film epitaxially grown on a (111)-oriented $Gd_3Ga_5O_{12}$ (GGG) substrate using off-axis sputtering, whose Gilbert damping α_{FM} can be measured as a reference using broadband FMR. The Gilbert damping $\alpha_{\mathrm{FM/NM}}$ in the micrometer-sized FM/NM area can be locally probed by comparing the LM resonance amplitude $\Delta A_{\mathrm{peak,\,FM/NM}}$ in the FM/NM bilayer area and $\Delta A_{\mathrm{peak,\,FM}}$ in the bare FM area. According to the previous discussion, we can use the

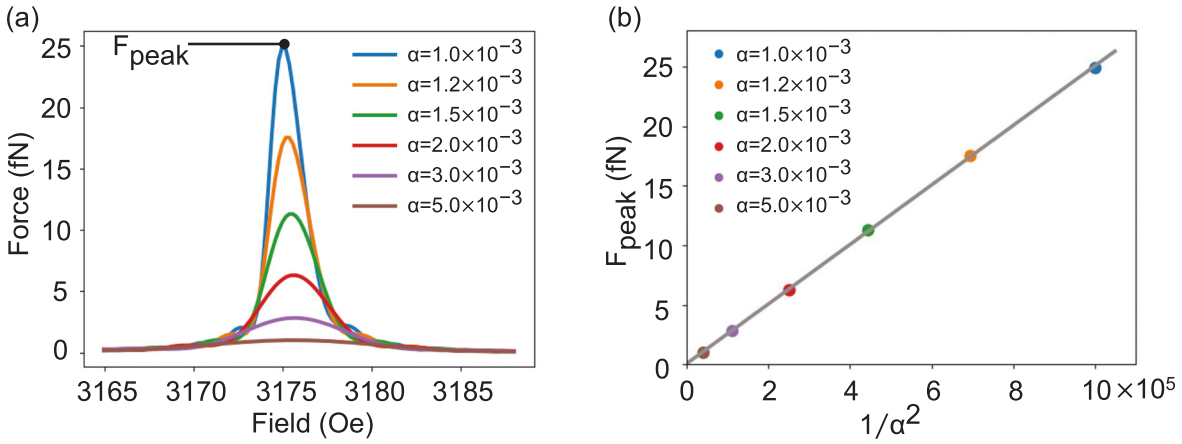

FIG. 2. Mumax3 simulation on $n = 1$ LM at different Gilbert damping and different probe height. (a) $|\vec{F}_{\mathrm{LM}}|(H)$ simulated around $H_{\mathrm{r,1}}$ with different Gilbert damping. F_{peak} is labeled for $\alpha = 1 \times 10^{-3}$ and it decreases as α increases. (b) The dependence of F_{peak} on α extracted from (a).

following equation to calculate the Gilbert damping in the FM covered by NM:

$$\alpha_{FM/NM} = \alpha_{FM} \times \sqrt{\Delta A_{peak,FM}/\Delta A_{peak,FM/NM}}. \quad (3)$$

The above-mentioned assumption that the effective Gilbert damping in a localized area equals the broadband FMR measured global Gilbert damping in the entire film requires the two-magnon scattering and inhomogeneous broadening contributions to be small.[22] The two-magnon scattering contribution can be easily excluded: we are doing the measurement with the magnetic field aligned normal to the sample plane, and the LMs have even lower resonance frequency than the uniform mode [Fig. 1(a)], so there is no degenerate magnon mode for LMs to scatter into. The effect of inhomogeneity is also excluded if the measurement is performed in a uniform area, which can be identified by an FMRFM scan. In order to confirm that there is no other intrinsic or extrinsic contribution that reduces the $\Delta A_{peak,FM}$, we resort to experimental examination of the soundness of the assumption.

As a proof of principle experiment, 5 μm × 20 μm heavy metal patterns a few nanometers thick (sample 1: 5 nm Au, sample 2: 3 nm and 6 nm Pt, and sample 3: 5 nm Ag) are deposited on a 20 nm YIG film using standard electron beam lithography (EBL) and sputtering [Fig. 3(a)]. We focus on the YIG/Au (5 nm) sample in the main text. In order to examine the accuracy of the scanned probe measurement, the YIG/Au (5 nm) sample we focus on also has another 1 mm ×1 mm × 5 nm Au pad patterned simultaneously on a separate area for the broadband FMR measurement. Figure 3(b) shows the RF frequency dependence of the linewidth obtained from broadband FMR measurements of both bare YIG and YIG/Au bilayer. We use $\gamma = 2\pi \times 27.958$ GHz/T for YIG to fit the broadband FMR result to Eq. (1) and get $\alpha_{YIG} = 1.09 \times 10^{-3}$ for a bare YIG film and $\alpha_{YIG/Au} = 1.29 \times 10^{-3}$ for the YIG/Au bilayer. The damping enhancement due to spin pumping $\alpha_{SP} = \alpha_{YIG/Au} - \alpha_{YIG} = 2.0 \times 10^{-4}$ is slightly smaller than that observed earlier,[23] possibly due to lower interface quality caused by our EBL process or the elimination of two magnon scattering in our field out-of-plane geometry.[24,25]

We now turn to the experimental demonstration of damping measurement using FMRFM. First, a line scan across the Au bar along the trace as indicated in Fig. 3(a) is obtained. The RF excitation frequency and power are fixed at 2 GHz and 1 dBm, respectively. After subtracting the background cantilever oscillation amplitude A_{off} measured when the applied field is away from the FMR resonance, we show only the change of signal amplitude ΔA due to the LM resonance in Fig. 3(c). Our focus is on the $n = 1$ LM resonance since it provides the highest spatial resolution.[26] In Fig. 3(c), the $n = 1$ LM resonance field $H_{r,1}$ is almost constant in the region $X < -4$ μm and $X > 4$ μm, indicating the constant probe height and high uniformity of the YIG film in the scan area. In the area -2 μm $< X < 1$ μm, a decrease in $H_{r,1}$ by ~8 Oe is resolved. Our previous studies of this interface-induced anisotropy find that a 5 nm Au overlayer induces a change of uniaxial anisotropy in 20 nm YIG[27] and that this anisotropy depends on both the overlayer material and the YIG thickness.[28] Therefore, the shift of $H_{r,1}$ is an indicator of the Au bar position.

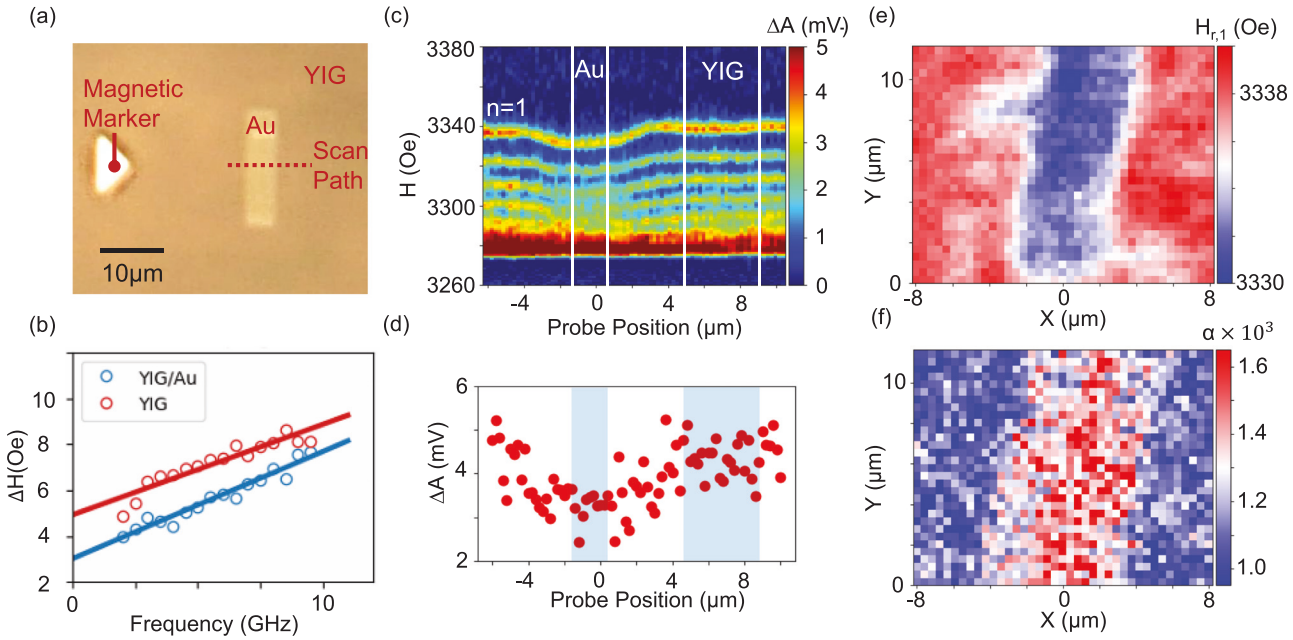

FIG. 3. Broadband FMR measurement and FMRFM spatially resolved imaging of YIG/Au spin pumping. (a) Optical picture of the 5 μm × 20 μm × 5 nm Au bar grown on a 20 nm YIG thin film. The magnetic marker is used to locate the position of the Au bar. (b) Broadband FMR measurement of the bare YIG and YIG/Au(5 nm) bilayer. (c) FMRFM scan along the scan path labeled as the red dashed line in (a). A background is subtracted to show the change of cantilever oscillation ΔA due to LMs. The shifting of the $n = 1$ LM resonance field $H_{r,1}$ is used to indicate the location of the Au bar. (d) The $n = 1$ LM resonance peak in (c) is fit to Eq. (4) and the symmetric Lorentzian amplitude is used as the indicator of the peak height and plotted to show its spatial variation. Reduction of ΔA is evident in -4 μm $< X < 3$ μm where the Au bar is located. (e) Two-dimensional mapping of $H_{r,1}$ clearly shows the shape of the Au bar. (f) Two-dimensional mapping of α shows the spin pumping induced Gilbert damping increase in the Au bar region.

To obtain ΔA_{peak} of the $n = 1$ LM in the FMRFM spectrum, we fit its resonance peak to an asymmetric Lorentzian line shape,[29]

$$\Delta A(H) = S\frac{\Delta H^2}{(H - H_{r,1})^2 + \Delta H^2} + D\frac{\Delta H(H - H_{r,1})}{(H - H_{r,1})^2 + \Delta H^2}, \quad (4)$$

where the first term is the symmetric Lorentzian function of field H centered at the resonance field $H_{r,1}$ with linewidth ΔH and amplitude S; the second term is the antisymmetric Lorentzian function with the same resonance field $H_{r,1}$ and linewidth ΔH but different amplitude D. We use the approximation $\Delta A_{\text{peak}} \approx S$ since the antisymmetric component D is small in our experiment. We plot the change of ΔA_{peak} along the line scan in Fig. 3(d). A decrease in ΔA_{peak} is evident in the region $-4\,\mu\text{m} < X < 3\,\mu\text{m}$. As our previous paper[27] showed, the decrease in ΔA_{peak} near the internal field step is partly due to the deformation of LMs. Therefore, we choose the uniform areas, where the probe is far away from the Au bar edge, to extract the spatial average of ΔA_{peak} in both bare YIG and the Au-covered YIG region. We obtain $\Delta A_{\text{peak, YIG/Au}} = 3.21\,\text{mV}$ in $-1.7\,\mu\text{m} < X < 0.4\,\mu\text{m}$, where the YIG/Au bilayer is located, and $\Delta A_{\text{peak,YIG}} = 4.39\,\text{mV}$ in $-4.6\,\mu\text{m} < X < 8.8\,\mu\text{m}$, the bare YIG area. Using Eq. (3) and $\alpha_{\text{YIG}} = 1.09 \times 10^{-3}$, we obtain a Gilbert damping in the YIG/Au bilayer of $\alpha_{\text{YIG/Au}} = 1.27 \times 10^{-3}$, close to the value measured by the broadband FMR. We note that RF field screening by a nanometer-thick metallic film[30,31] could also potentially lead to ΔA_{peak} reduction. To address this issue, we replace Au with Ag and perform the same measurement (sample 3). Compared to Au, Ag exhibits negligible spin pumping[11] but has similar conductivity. We patterned a 5 nm Ag bar on 20 nm YIG and find no observable change in ΔA_{peak}, demonstrating RF field screening is negligible.

We perform two-dimensional mapping using the $n = 1$ LM in the range $-8\,\mu\text{m} < X < 8\,\mu\text{m}$ and $0\,\mu\text{m} < Y < 11\,\mu\text{m}$ with an ~500 nm step size using the same RF excitation frequency and power. At each position, $H_{r,1}$ and ΔA_{peak} are simultaneously extracted using Eqs. (3) and (4). Figure 3(e) shows the spatial variation of $H_{r,1}$, where the shape of the Au bar is clearly resolved as the area of blue color, indicating an ~8 Oe decrease in $H_{r,1}$ relative to the bare YIG shown as the red color. We use the spatial average of ΔA_{peak} in the bare YIG area, $\overline{\Delta A}_{\text{peak,YIG}}$, as the reference and calculate the Gilbert damping at each location using $\alpha(x, y) = \alpha_{\text{YIG}} \times \sqrt{\overline{\Delta A}_{\text{peak,YIG}}/\Delta A(x, y)}$, where $\alpha_{\text{YIG}} = 1.09 \times 10^{-3}$. The spatial mapping of $\alpha(x, y)$ is shown in Fig. 3(f), which clearly resolves the increase in Gilbert damping in the YIG/Au bilayer region.

We further obtain one-dimensional FMRFM scans at different RF frequencies and use the same analysis to obtain the Gilbert damping in the YIG/Au bilayer. Figure 4 shows the calculated $\alpha_{\text{YIG/Au}}$ at all frequencies measured; we find their average value of $\overline{\alpha}_{\text{YIG/Au}} = 1.36 \times 10^{-3}$, reasonably close to the values measured by broadband FMR and reported in the literature.[23] This indicates that our assumption that the effective damping of a localized mode in bare YIG equals the Gilbert damping of bare YIG measured globally is sound.

The clearly resolved Gilbert damping variation of order 2.0×10^{-4} corresponds to a difference in linewidth $\Delta H_{\text{YIG/Au}} - \Delta H_{YIG} \approx 0.16\,\text{Oe}$ at $f = 2\,\text{GHz}$. This high sensitivity is achievable because of the extreme force sensitivity of the FMRFM. The minimum detectable force in our FMRFM is $F_{\text{min}} \approx 2\,\text{fN}$, smaller than the

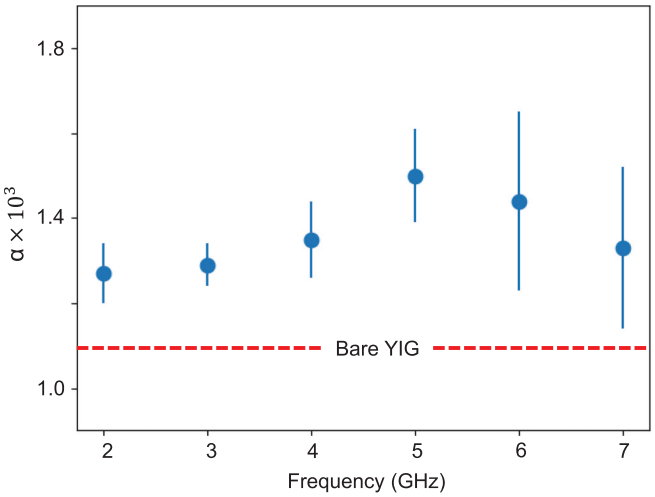

FIG. 4. RF Frequency dependence of Gilbert damping measured using FMRFM. The red dashed line represents the Gilbert damping of bare YIG $\alpha_{\text{YIG}} = 1.09 \times 10^{-3}$ measured using broadband FMR. Blue data points and error bar represent $\alpha_{\text{YIG/Au}}$ and its standard deviation measure from one-dimensional FMRFM scans at different RF frequencies.

modification of F_{peak} due to the Gilbert damping difference $\Delta\alpha = 2.0 \times 10^{-4}$. Assuming the resonance cone angle $\theta_{0,\text{YIG}} = 2°$ in bare YIG, the resonance cone angle will change to $\theta_{0,\text{YIG/Au}} = 2 \times \alpha_{\text{YIG}}/\alpha_{\text{YIG/Au}} \approx 1.7°$ when the probe is over the YIG/Au bilayer. This reduction of resonance cone angle will lead to ~7 fN change of F_{peak} indicated by the blue dashed line in Fig. 1(e), which is greater than F_{min}. The value of F_{min} is determined by the FMRFM working temperature and the cantilever quality factor.

Although the data in Fig. 4 cannot rule out a slight frequency dependence, it is most likely due to measurement error, this experiment shows the possibility of studying the relation between relaxation and resonance frequency. Improving our control over the interferometer setpoint and reducing spurious drive of the cantilever by the RF field will improve the signal to noise ratio and improve our ability to resolve the delicate damping frequency dependence.

In conclusion, we theoretically proposed, numerically examined, and experimentally demonstrated an alternative method of local Gilbert damping measurement using the LM resonance amplitude in FMRFM. Using this measurement scheme, we report the nanoscale imaging of Gilbert damping spatial variation in a FM. This technique is useful when studying spin dynamics in insulating FM thin films and FM/NM bilayers, especially when the NM layer has a small lateral size such as van der Waals materials. The capability to measure Gilbert damping at a single RF excitation frequency also opens the possibility to study the frequency dependence of magnon relaxation due to interfacial spin transport.

See the supplementary material for the illustration of variational calculation, analytical derivation of Eq. (2), MuMax3 simulations setup, FMRFM experimental data and fitting, experiments on other samples, and calculation of FMRFM force sensitivity.

This work was primarily supported by the Center for Emergent Materials (CEM), an NSF-funded MRSEC under Award

No. DMR-2011876. Y.C. acknowledges partial support from the Department of Energy (DOE), Office of Science, Basic Energy Sciences, under Grant No. DE-SC0001304. Fabrication and some characterization were performed in the Ohio State University NanoSystems Laboratory.

DATA AVAILABILITY

The data that support the findings of this study are available from the corresponding author upon reasonable request.

REFERENCES

[1]M. S. Grinolds, S. Hong, P. Maletinsky, L. Luan, M. D. Lukin, R. L. Walsworth, and A. Yacoby, Nat. Phys. **9**, 215 (2013).
[2]D. Rugar, H. J. Mamin, M. H. Sherwood, M. Kim, C. T. Rettner, K. Ohno, and D. D. Awschalom, Nat. Nanotechnol. **10**, 120 (2015).
[3]C. H. Du, T. van der Sar, T. X. Zhou, P. Upadhyaya, F. Casola, H. L. Zhang, M. C. Onbasli, C. A. Ross, R. L. Walsworth, Y. Tserkovnyak, and A. Yacoby, Science **357**, 195 (2017).
[4]P. Willke, K. Yang, Y. Bae, A. J. Heinrich, and C. P. Lutz, Nat. Phys. **15**, 1005 (2019).
[5]K. Yang, W. Paul, S. H. Phark, P. Willke, Y. Bae, T. Choi, T. Esat, A. Ardavan, A. J. Heinrich, and C. P. Lutz, Science **366**, 509 (2019).
[6]D. Rugar, R. Budakian, H. J. Mamin, and B. W. Chui, Nature **430**, 329 (2004).
[7]P. E. Wigen, M. L. Roukes, and P. C. Hammel, *Spin Dynamics in Confined Magnetic Structures III* (Springer, 2006), Vol. 101, p. 105.
[8]I. Lee, Y. Obukhov, G. Xiang, A. Hauser, F. Yang, P. Banerjee, D. V. Pelekhov, and P. C. Hammel, Nature **466**, 845 (2010).
[9]R. Adur, C. H. Du, H. L. Wang, S. A. Manuilov, V. P. Bhallamudi, C. Zhang, D. V. Pelekhov, F. Y. Yang, and P. C. Hammel, Phys. Rev. Lett. **113**, 176601 (2014).
[10]A. Hamadeh, O. D. Kelly, C. Hahn, H. Meley, R. Bernard, A. H. Molpeceres, V. V. Naletov, M. Viret, A. Anane, V. Cros, S. O. Demokritov, J. L. Prieto, M. Munoz, G. de Loubens, and O. Klein, Phys. Rev. Lett. **113**, 197203 (2014).
[11]H. Wang, C. Du, Y. Pu, R. Adur, P. C. Hammel, and F. Yang, Phys. Rev. Lett. **112**, 197201 (2014).
[12]S. Singh, A. K. Patra, B. Barin, E. del Barco, and B. Ozyilmaz, IEEE Trans. Magn. **49**, 3147 (2013).
[13]J. B. S. Mendes, O. A. Santos, L. M. Meireles, R. G. Lacerda, L. H. Vilela-Leao, F. L. A. Machado, R. L. Rodriguez-Suarez, A. Azevedo, and S. M. Rezende, Phys. Rev. Lett. **115**, 226601 (2015).
[14]S. Dushenko, H. Ago, K. Kawahara, T. Tsuda, S. Kuwabata, T. Takenobu, T. Shinjo, Y. Ando, and M. Shiraishi, Phys. Rev. Lett. **116**, 166102 (2016).
[15]D. MacNeill, G. Stiehl, M. Guimaraes, R. Buhrman, J. Park, and D. Ralph, Nat. Phys. **13**, 300 (2017).
[16]J. B. S. Mendes, O. A. Santos, T. Chagas, R. Magalhaes-Paniago, T. J. A. Mori, J. Holanda, L. M. Meireles, R. G. Lacerda, A. Azevedo, and S. M. Rezende, Phys. Rev. B **99**, 214446 (2019).
[17]G. N. Kakazei, P. E. Wigen, K. Y. Guslienko, V. Novosad, A. N. Slavin, V. O. Golub, N. A. Lesnik, and Y. Otani, Appl. Phys. Lett. **85**, 443 (2004).
[18]G. Z. Wu, S. P. White, W. T. Ruane, J. T. Brangham, D. V. Pelekhov, F. Y. Yang, and P. C. Hammel, Phys. Rev. B **101**, 184409 (2020).
[19]O. Klein, G. Loubens, V. V. Naletov, F. Boust, T. Guillet, H. Hurdequint, A. Leksikov, A. N. Slavin, V. S. Tiberkevich, and N. Vukadinovic, Phys. Rev. B **78**, 144410 (2008).
[20]O. Klein, V. Charbois, V. V. Naletov, and C. Fermon, Phys. Rev. B **67**, 220407 (2003).
[21]A. Vansteenkiste, J. Leliaert, M. Dvornik, M. Helsen, F. Garcia-Sanchez, and B. van Waeyenberge, AIP Adv. **4**, 107133 (2014).
[22]X. Y. Lu, L. J. Atkinson, B. Kuerbanjiang, B. Liu, G. Q. Li, Y. C. Wang, J. L. Wang, X. Z. Ruan, J. Wu, R. F. L. Evans, V. K. Lazarov, R. W. Chantrell, and Y. B. Xu, Appl. Phys. Lett. **114**, 192406 (2019).
[23]J. T. Brangham, K.-Y. Meng, A. S. Yang, J. C. Gallagher, B. D. Esser, S. P. White, S. Yu, D. W. McComb, P. C. Hammel, and F. Yang, Phys. Rev. B **94**, 054418 (2016).
[24]R. Arias and D. L. Mills, Phys. Rev. B **60**, 7395 (1999).
[25]L. J. Zhu, D. C. Ralph, and R. A. Buhrman, Phys. Rev. Lett. **123**, 057203 (2019).
[26]I. Lee, Y. Obukhov, A. J. Hauser, F. Y. Yang, D. V. Pelekhov, and P. C. Hammel, J. Appl. Phys. **109**, 07D313 (2011).
[27]G. Wu, S. P. White, W. Ruane, J. T. Brangham, D. Pelekhov, F. Yang, and P. C. Hammel (submitted).
[28]A. J. Lee, A. S. Ahmed, J. Flores, S. D. Guo, B. B. Wang, N. Bagues, D. W. McComb, and F. Y. Yang, Phys. Rev. Lett. **124**, 107201 (2020).
[29]M. Harder, Y. S. Gui, and C. M. Hu, Phys. Rep. **661**, 1 (2016).
[30]M. Bailleul, Appl. Phys. Lett. **103**, 192405 (2013).
[31]I. S. Maksymov and M. Kostylev, J. Appl. Phys. **116**, 173905 (2014).